CrystEngComm

PAPER

View Article Online
View Journal | View Issue

Cite this: *CrystEngComm*, 2015, **17**, 2168

Preparation, optical property and field-effect mobility investigation of stable white-emissive doped organic crystal†

Huan Wang,*[a] Yang Zhao,[a] Zengqi Xie,[b] Hui Shang,*[c] Huaiyuan Wang,[a] Feng Li[d] and Yuguang Ma*[b]

Received 19th December 2014,
Accepted 1st February 2015

DOI: 10.1039/c4ce02501f

www.rsc.org/crystengcomm

Different from most reported white-light-emission amorphous doped organic films obtained through precisely controlling a very low and specific doping concentration usually smaller than 1%, tetracene (Tc) and pentacene (Pc) doubly doped *trans*-1,4-distyrylbenzene (DSB) crystals (DSB⊂Tc–Pc), prepared by physical vapor transport (PVT) method presented a white-light emission with approximately 10 mol% dopant concentrations (DSB : Tc : Pc = 20 : 1 : 0.9). This is attributed to the intermolecular strong arene–arene interactions inducing a cross donor–acceptor transition dipole arrangement, that is efficient in restricting energy transfer. The time-resolved fluorescence properties have been investigated in detail to analyze the energy transfer process between DSB and Tc/Pc molecules in the DSB⊂Tc–Pc crystal. In addition, the maintenance of structural ordering of the white-emissive doped crystal has been verified by atomic force microscopy (AFM) and X-ray diffraction (XRD), which benefits the carrier transport; the hole and electron field-effect mobility were measured as 1.62×10^{-2} and 2.15×10^{-4} cm^2 V^{-1} s^{-1}, respectively. Also due to the intermolecular highly ordered arrangement, the DSB⊂Tc–Pc crystal exhibits ideal and stable white-light emission with CIE coordinates approaching to (0.33, 0.33) even under high pumping laser energy excitation. These results indicate the stable white-emissive doped organic crystals can be prepared by PVT and has high potential of realizing white electroluminescence based on the device configurations of light-emitting diodes or field-effect transistors.

Introduction

Organic crystals constructed by π-conjugated molecules have attracted great attention in the field of organic optoelectronic materials,[1–4] of which the defined structures provide a model to investigate the relationship between molecular stacking modes and optoelectronic performance (luminescence and carrier mobility).[5,6] Additionally, the superiorities of organic crystals such as high thermal stability and high carrier mobility make them attractive candidates for optoelectronic devices such as optically pumped lasers,[7–9] field-effect transistors,[10–12] in electroluminescence,[13–15] and photovoltaic cells.[16–18] Doped organic molecular crystals have received much attention since the 1970s and stimulated emissions in some systems were subsequently observed.[19,20] Doping has the advantage for tuning the emission color and decreasing the absorption loss *via* energy transfer. For white-emissive doped organic crystal growth, the host–guest system of two cyan–orange components or three blue–green–red components is usually considered. Yao and coworkers successfully fabricated white luminescent nanowires by merely blending a blue dye with an orange one through the adsorbent-assisted physical vapor deposition (PVD) method.[21] Notably, micro- or nano-size organic crystals lack structural definition and this limits their application in optoelectronic devices. Thus, large-size (millimeter scale) crystals are in high demand for the fabrication of devices, which can endure high current density up to several kA cm^{-2} without luminescence efficiency roll-off[22,23] and will open a realistic route towards organic bright lighting devices.

Recently, high-luminescence and large-size doped organic crystals with structural-order retention have been prepared by physical vapor transport (PVT) method based on *trans*-1,4-distyrylbenzene (DSB) as the host and tetracene (Tc) or pentacene (Pc) as the guest.[24] Tc doped DSB crystals (abbreviated

[a] *College of Chemistry and Chemical Engineering, Northeast Petroleum University, Daqing, 163318, PR China. E-mail: wanghuan83214@gmail.com; Fax: (+86)459 6504154; Tel: (+86)459 6504154*
[b] *State Key Laboratory of Luminescent Materials and Devices, Institute of Polymer Optoelectronic Materials and Devices, South China University of Technology, Guangzhou, 510640, PR China. E-mail: ygma@scut.edu.cn*
[c] *Department of Physics, Graduate School of Science, Tohoku University, Sendai, 980-8578, Japan. E-mail: shanghui0625@gmail.com*
[d] *State Key Laboratory of Supramolecular Structure and Materials, Jilin University, Changchun, 130012, PR China*

† Electronic supplementary information (ESI) available: Details of chromatograph analysis for the white-emissive DSB⊂Tc–Pc crystals, the emission spectra of singly doped crystals, the data of pure DSB crystal-based field-effect transistors and the color stability test of the doped thin film excited with different pumping laser energy. See DOI: 10.1039/c4ce02501f

as DSB⊂Tc crystal) and Pc doped DSB crystals (abbreviated as DSB⊂Pc crystal) present green and red light emissions, respectively; and the doping concentrations of Tc or Pc molecules can approach 8% which is mainly attributed to the structural comparability of host and guest molecules and their similar 'herringbone' type molecular stacking in crystals.[25–27] Subsequently, it has been demonstrated that such high doping concentration can be viable for optoelectronic devices due to the mutually perpendicular transition dipole orientations between host and guest, which results in a small value of orientation factor κ^2 and thereby reduces the efficiency of resonance energy transfer (RET).[28] Because a cross dipole arrangement between the donor and acceptor molecules could be efficient to restrict the energy transfer process and then to realize a partial energy transfer even at high doping concentrations, it will facilitate preparation of a white-light emissive organic crystal overcoming the concentration-sensitivity problem and having good color reproducibility and stability.

In this paper, Tc and Pc as green and red dopants respectively, were simultaneously doped into the DSB crystal (abbreviated as DSB⊂Tc–Pc crystal) by the PVT method. Combined with the crystal growth thermodynamic characteristics,[29] the white-emissive DSB⊂Tc–Pc crystal with a specific mol ratio of host to guest molecules (DSB : Tc : Pc = 20 : 1 : 0.9) has been obtained under conditions of suitable temperature. The host DSB and the guest Tc/Pc are all show linear and planar molecular configurations and their intermolecular strong arene–arene interactions induce the cross dipole arrangement between DSB and Tc/Pc in the doped crystal formation process which is inefficient for energy transfer, thus allowing high doping concentrations (Tc and Pc added up to nearly 10%). The energy transfer occurring not only from the donor DSB to the acceptors Tc and Pc but also from the acceptor Tc to the acceptor Pc has been verified by time-resolved fluorescence. The DSB⊂Tc–Pc crystal maintains the structural ordering as proved by X-ray diffraction (XRD) and atomic force microscopy (AFM) analysis; and the crystal mobilities deduced from field-effect transistor (FET) measurements for holes and electrons are 1.62×10^{-2} and 2.15×10^{-4} cm^2 V^{-1} s^{-1}, respectively, of which the hole mobility is comparable to that of pure DSB crystal. Based on the highly ordered arrangement between host–guest molecules, the white-emissive DSB⊂Tc–Pc crystal under high pumping laser energy excitation still exhibits a good color stability with the Commission International del'Eclairage (CIE) coordinates approaching to an ideal white light (0.33, 0.33). The preliminary analyses on the optoelectronic properties of the white-emissive DSB⊂Tc–Pc crystal prepared by PVT will guide us to design and fabricate stable organic white-light crystal devices.

Experimental section

UV-vis absorption and fluorescence spectra were recorded using UV-3100 and RF-5301PC spectrophotometers, respectively. The atomic force microscope (AFM) images were recorded on a Seiko SPA 400 with an SPI 3800 probe station in tapping mode (dynamic force mode). Commercially available Si cantilevers with a force constant of 20 N m^{-1} were used. The wide-angle X-ray diffraction was measured with a Rigaku X-ray diffractometer (D/Max-rA, using Cu-Kα radiation of wavelength 1.542 Å), and in the test the slice crystal sample was rested parallel to the single-crystal Si substrate.

High-performance liquid chromatography (LC-20A) was used to analyze the component content of the doped crystals. C18 (octadecylsilyl, ODS) was used as the packing material in the column, and the column temperature was controlled at 40 °C, and an ultraviolet detector (254 nm) was employed. A mixed solution of CH_3OH (80 vol%) and H_2O (20 vol%) was used as the flow phase and the flow rate was controlled as 1 mL min^{-1}. All the detected components could be dissolved in tetrahydrofuran (THF).

Time-resolved fluorescence measurements were performed using a time-correlated single-photon counting (TCSPC) system under right-angle sample geometry. A 379 nm picosecond diode laser (Edinburgh Instruments EPL375, repetition rate 20 MHz) was used to excite the sample. The emission was detected by a photomultiplier tube (Hamamatsu H5783p) and a TCSPC board (Becker&Hickel SPC-130). The instrument response function (IRF) is about 220 ps. All the measurements were performed at room temperature (22 °C).

For the pumping laser excitation test, sliced crystal specimens adhered to the quartz substrate were irradiated by the third harmonic (355 nm) of a Nd:YAG (yttrium-aluminum-garnet) laser at a repetition rate of 10 Hz and pulse duration of about 10 ns. The energy of the pumping laser was adjusted by using calibrated neutral density filters. The beam was focused into a stripe whose shape is adjusted to 4 × 0.5 mm through using a cylindrical lens and a slit. The edge emission of the crystals was detected using a charge-coupled-device (CCD) fiber spectrograph. All the measurements were carried out at room temperature under ambient conditions.

Crystal FET fabrications: a 200 nm-thick SiO_2 layer on a highly doped silicon wafer was used as an insulator. A 100 nm-thick poly(methylmethacrylate) (PMMA) layer was spin coated from a toluene solution (30 mg mL^{-1}) onto the wafer. After the PMMA deposition, the substrates were maintained overnight in an oven at 70 °C and were subsequently annealed at 100 °C for 3 h under a N_2 atmosphere. Next, the crystal was carefully placed on the substrate. The 200 nm-thick top-contact gold or calcium electrodes were thermally evaporated on the crystal surface at a rate of 0.1–0.2 nm s^{-1} through a shadow mask under a background pressure of 1×10^{-6} mbar. The channel length and width were checked with an optical microscope. The FET measurements were carried out using a semiconductor parameter analyzer HP4155C (Agilent Technologies) in a glovebox without exposing the substrate to air.

Tetracene and pentacene, purchased from J&K ACROS (98%), were purified by sublimation a few times before use. *trans*-1,4-Distyrylbenzene was synthesized and purified as referred to in our previous work.[30]

Results and discussion

1. Preparation of white-emissive DSB⊂Tc–Pc crystals

The energy transfer efficiency in a donor–acceptor system is strongly dependent on the transition dipole arrangement between the donor and acceptor molecules which can be described by the orientation factor κ^2, ranging from 0 to 4 (Fig. 1a); for instance when the two dipoles are perpendicular one to another, the orientation factor κ^2 is equal to zero, and the energy transfer process will be forbidden, as prediction of the theory developed by Förster more than 60 years ago.[31] DSB, a brick-like conjugated molecule with dipole transition along its long molecular direction as shown in Fig. 1b, tends to form 'herringbone' type stacking in crystals and the crystal shows intense blue emission with photoluminescence quantum efficiency as high as 70%.[25,32] Both Tc and Pc possess quite similar molecular configurations and also molecular stacking modes as that of DSB;[26,33,34] However, their dipole transition direction is totally different, that is along the short molecular axes (Fig. 1b).[35,36] Meanwhile, Tc and Pc show green and red emission in dilute solutions, respectively; and their absorption spectra have some overlap with the DSB crystal emission spectrum shown in Fig. 1c, which means the preparation of white-emissive doped crystals with DSB as the energy donor and Tc/Pc as the energy acceptors is feasible. The spectra data are summarized in Table 1.

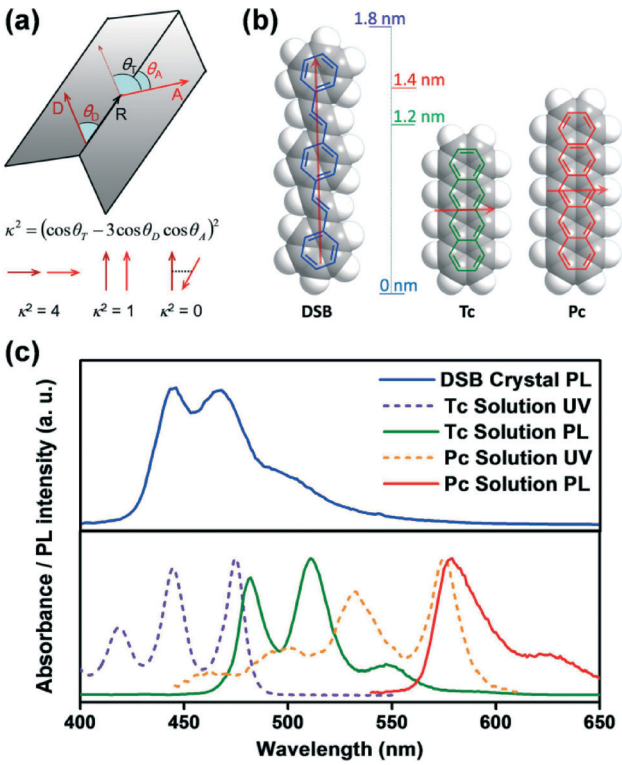

Fig. 1 (a) Spatial orientation of donor and acceptor dipoles (red arrows) and the relationship with orientation factor κ^2. $\kappa^2 = (\cos\theta_T - 3\cos\theta_D\cos\theta_A)^2$, where θ_D is the angle between the donor dipole and R (the vector from the donor to the acceptor). θ_A is the angle between the acceptor dipole and R. θ_T is the angle between donor and acceptor dipoles. (b) Molecular structures of DSB, Tc and Pc. The dipole transition direction of DSB is along its long molecular axis, while those of Tc and Pc are along their short axes. (c) The emission spectrum of the DSB crystal (top) and absorption and emission spectra of Tc and Pc solutions in chloroform (bottom).

The crystal growth apparatus was reported in our previous work as shown in Fig. 2a.[37] Pc, DSB and Tc were placed sequentially in the source zone of the apparatus where the temperature gradient varied from 250 to 150 °C according to the sublimation temperatures of the materials. The sublimed molecules were transported with a carrier gas (Ar, 99.999%), and then the crystals grew in the growth zone. After two or three days of stable growth, large-size slice crystals emitting white light under the excitation of ultraviolet light were formed hanging inside of the growth tube.

The emission spectrum of the white-emissive DSB⊂Tc–Pc crystal is shown in Fig. 2b (inset is the corresponding optical photograph of a crystal under a UV-lamp), where the 0–0/0–1 transition emissions of DSB, Tc and Pc are at *ca.* 444/467, 497/531 and 603/654 nm, respectively. The emission peaks of Tc and Pc in the DSB⊂Tc–Pc crystal show about 20–30 nm red shifts relative to those in the solution, which may be caused by the conjugated effect of Tc/Pc with the surrounding DSB molecules. Fig. 2c shows the CIE coordinate of (0.36, 0.37) corresponding to the emission of the DSB⊂Tc–Pc crystal shown in Fig. 2b, approaching to an ideal white light (0.33, 0.33); and the mol ratio of host to guest molecules (DSB : Tc : Pc = 20 : 1 : 0.9) was estimated by chromatograph analysis (see ESI† for the details).

In the white-emissive doubly doped DSB⊂Tc–Pc crystal, the total dopant concentrations including both Tc and Pc up to approximately 10% are attributed to their similar linear and planar molecular configurations to that of DSB; an energy transfer occurs partially from donor to acceptor as a result of their almost mutually perpendicular transition dipole arrangement, which is further discussed below.

2. Time-resolved fluorescence to analyze the energy transfer process

Fig. 3a shows the photoluminescence decay curves of DSB⊂Tc crystals with two different mol ratios (DSB : Tc = 33 : 1, 18 : 1), and the white-emissive doubly doped DSB⊂Tc–Pc crystal (DSB : Tc : Pc = 20 : 1 : 0.9) monitored at the emission wavelength of 444 nm. The decay time of the donor DSB in the above three doped crystals are 1.49, 1.04 and 0.11 ns, respectively. Obviously, the decay time of DSB in the DSB⊂Tc–Pc crystal is much shorter than that in the DSB⊂Tc

Table 1 Summaries of the absorption and emission wavelengths of DSB crystal and Tc/Pc solutions

	Absorption wavelength/nm			Emission wavelength/nm		
Material	0–2	0–1	0–0	0–0	0–1	0–2
DSB crystal	—	—	—	444	467	500
Tc solution	419	445	475	482	511	549
Pc solution	496	532	575	579	625	—

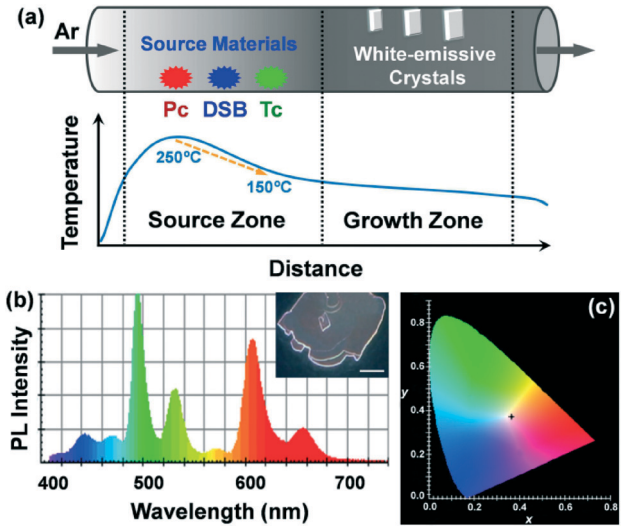

Fig. 2 (a) Schematics of the apparatus for the growth of doped crystals by the physical vapor transport method. The temperature in the apparatus is controlled as shown in the bottom. The temperatures of Pc, DSB and Tc heated for the sublimation are controlled at 250, 210 and 150 °C, respectively, in the source zone; and the white-emissive crystals were obtained in the growth zone. (b) The emission spectrum of the DSB⊂Tc–Pc crystal (inset is the corresponding optical photograph of a crystal under the UV-lamp; scale bar is 1 mm). (c) CIE chromaticity diagram marked as the cross (0.36, 0.37) corresponding to the crystal emission shown in Fig. 2b.

crystals although the mol ratio of DSB to Tc (20 : 1) in the DSB⊂Tc–Pc crystal lies between 33 : 1 and 18 : 1. That means the energy transfer occurs not only from the donor DSB to the acceptor Tc but also from the donor DSB to the acceptor Pc in the white-emissive doubly doped crystal. Fig. 3b shows the photoluminescence decay curves of DSB⊂Tc crystals with two different mol ratios (DSB : Tc = 33 : 1, 18 : 1), and the white-emissive doubly doped DSB⊂Tc–Pc crystal (DSB : Tc : Pc = 20 : 1 : 0.9), monitored at an emission wavelength of 531 nm. The decay time of the acceptor Tc in the above three doped crystals are 10.01, 14.51 and 2.37 ns, respectively. As can be seen, the decay time of Tc in the DSB⊂Tc–Pc crystal is largely decreased to 2.37 ns compared with that in the DSB⊂Tc crystals, indicating efficient energy transfer from Tc to Pc in the white-emissive doubly doped crystal. Fig. 3c shows the photoluminescence decay curves of DSB⊂Pc crystals with two different mol ratios (DSB : Pc = 28 : 1, 16 : 1), and the white-emissive doubly doped DSB⊂Tc–Pc crystal (DSB : Tc : Pc = 20 : 1 : 0.9) monitored at the emission wavelength of 608 nm. The decay time of the acceptor Pc in the above three doped crystals are 6.92, 8.29 and 8.06 ns, respectively. This indicates the decay time of Pc in the doped crystals is proportional to its doping concentration and the acceptor molecules are embedded in the DSB crystal with approximately uniform dispersion. A summary of transient photoluminescence decay time for the above systems is given in Table 2. The emission properties of DSB⊂Tc (DSB : Tc = 33 : 1, 18 : 1) and DSB⊂Pc (DSB : Pc = 28 : 1, 16 : 1) crystals are given in the ESI.†

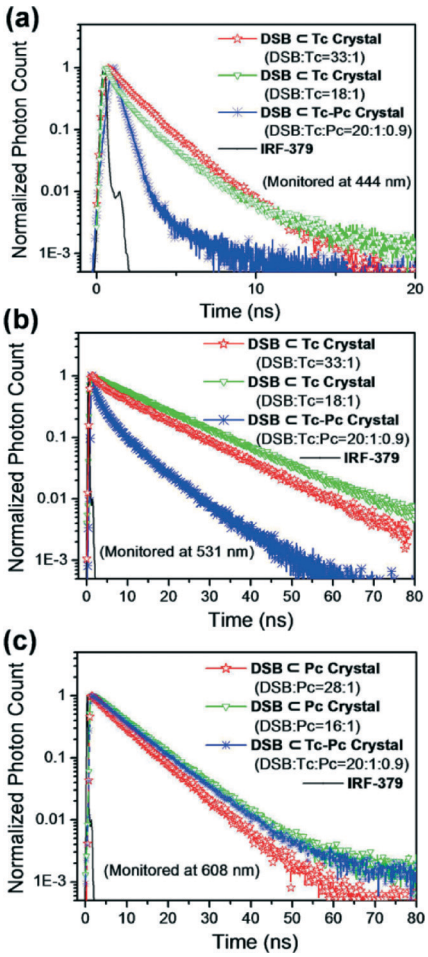

Fig. 3 Time-resolved fluorescence decay curves of the white-emissive doubly doped DSB⊂Tc–Pc crystal (DSB : Tc : Pc = 20 : 1 : 0.9) monitored at different emission wavelengths. The decay curves of DSB⊂Tc crystals (DSB : Tc = 33 : 1, 18 : 1) and DSB⊂Pc crystals (DSB : Pc = 28 : 1, 16 : 1) with different mol ratios are also shown for comparison: (a) λ_{em} = 444 nm; (b) λ_{em} = 531 nm; (c) λ_{em} = 608 nm.

Based on the above analyses, it is demonstrated that the energy transfer occurs not only from the donor DSB to the acceptors Tc and Pc but also from the acceptor Tc to the acceptor Pc in the white-emissive doubly doped DSB⊂Tc–Pc crystal. Herein, the stacking mode between molecules determines the host–guest intermolecular dipole orientation, impacting on the energy transfer process in the DSB⊂Tc–Pc crystal.

3. Morphology and structure of the white-emissive DSB⊂Tc–Pc crystal

Fig. 4a shows the AFM height image at a surface area of the DSB⊂Tc–Pc crystal (DSB : Tc : Pc = 20 : 1 : 0.9) and step-like morphology is observed. From the cross-section analyses, the average height of steps observed on the crystal surface is about 1.78 nm. Fig. 4b shows the diffraction patterns of wide-angle X-ray diffraction (XRD) on the above mentioned slice doped crystal and comparatively pure DSB crystal. As

Table 2 Decay data of the white-emissive doubly doped DSB⊂Tc–Pc crystal (DSB : Tc : Pc = 20 : 1 : 0.9), DSB⊂Tc crystals (DSB : Tc = 33 : 1, 18 : 1) and DSB⊂Pc crystals (DSB : Pc = 28 : 1, 16 : 1) with different mol ratios monitored at emission wavelengths of 444, 531 and 608 nm, respectively

Crystal	Decay time τ/ns	Percentage (%)	Mean lifetime τ/ns	λ_{em}/nm
DSB⊂Tc crystal (DSB : Tc = 33 : 1)	2.28 1.04	36.09 63.91	1.49	444
DSB⊂Tc crystal (DSB : Tc = 18 : 1)	1.94 0.50	34.47 65.20	1.04	
DSB⊂Tc–Pc crystal (DSB : Tc : Pc = 20 : 1 : 0.9)	0.79 0.09	2.67 97.33	0.11	
DSB⊂Tc crystal (DSB : Tc = 33 : 1)	13.23 2.110	71.07 28.93	10.01	531
DSB⊂Tc crystal (DSB : Tc = 18 : 1)	14.51	100	14.51	
DSB⊂Tc–Pc crystal (DSB : Tc : Pc = 20 : 1 : 0.9)	7.30 0.86	23.39 76.61	2.37	
DSB⊂Pc crystal (DSB : Pc = 28 : 1)	6.92	100	6.92	608
DSB⊂Pc crystal (DSB : Pc = 16 : 1)	8.29	100	8.29	
DSB⊂Tc–Pc crystal (DSB : Tc : Pc = 20 : 1 : 0.9)	8.06	100	8.06	

can be seen, the diffraction peaks occur equidistantly with 2θ, and the diffraction peaks are very sharp, so the doped crystal has an ordered layer structure. The lattice parameters of pure DSB were reported by Wu *et al.*:[25] a = 5.87 Å, b = 7.70 Å, c = 34.87 Å. The herringbone arrangement of DSB molecules in the crystal was recognized in previous work.[38,39] According to the Bragg equation $2d \sin\theta = n\lambda$, the thickness of one molecular layer of DSB⊂Tc–Pc crystal is calculated to be 1.76 nm, which corresponds to the one-step height of the doped crystal in the AFM image.

The results of AFM morphology and X-ray diffraction pattern suggest that the DSB⊂Tc–Pc crystal has a layer-by-layer structure and each layer corresponds to a molecular monolayer. Therefore, the structural ordering of the DSB⊂Tc–Pc crystal is retained after doping a certain quantity of Tc and Pc molecules into the DSB matrix, which means doped guest molecules may replace the locations of original host molecules in the crystal lattice. Doping Tc and Pc into DSB crystal leads a slightly larger layer space (one molecular layer thickness in a pure DSB crystal is 1.72 nm), attributed to the disturbance of the intrinsic DSB crystal lattices caused by the embedment of doped molecules. Importantly, both DSB as the host molecules and Tc/Pc as the guest molecules are all in linear configurations and the molecules in the crystals are arranged in similar 'herringbone' type structure in the *ab* plane, where edge-to-face arene–arene interactions are much stronger than intermolecular interactions along the *c* axis direction; thus, the cross transition dipole arrangement between DSB and Tc/Pc molecules is fixed when the layer-by-layer structure is formed.

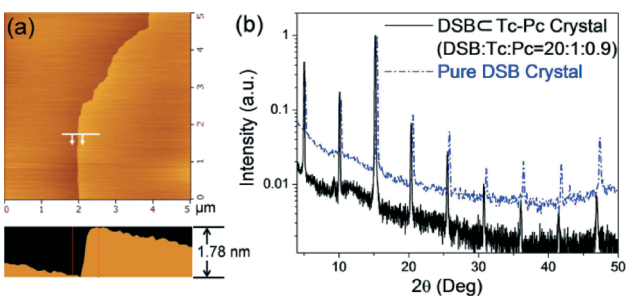

Fig. 4 (a) AFM height image of the surface of a DSB⊂Tc–Pc crystal (DSB : Tc : Pc = 20 : 1 : 0.9) and its enlarged sectional analysis. (b) Wide-angle X-ray diffraction patterns of DSB⊂Tc–Pc crystal (DSB : Tc : Pc = 20 : 1 : 0.9) and pure DSB crystal.

Fig. 5 shows the schematics of the proposed molecular stacking and energy transfer process in the white-emissive DSB⊂Tc–Pc crystal. The energy is usually considered to transfer along the direction of molecular transition dipole from donor to acceptor. When RET is 50% efficient, the donor–acceptor distance is equal to the Förster distance R_0,[40] which is described by the relation:

$$R_0^6 = \frac{9000(\ln 10)\kappa^2\phi_D}{128\pi^5 n^4 N_A} J_C$$

where φ_D is the quantum yield of the donor in the absence of acceptor, n is the refractive index of the medium, N_A is Avogadro's number, J_C is the spectral overlap integral calculated as $J_C = \int_0^\infty F_D(\lambda)\varepsilon_A(\lambda)\lambda^4\, d\lambda$. $F_D(\lambda)$ is the normalized donor emission spectrum, and $\varepsilon_A(\lambda)$ is the acceptor molar extinction coefficient. Notably, as is evident in the above equation, the Förster distance R_0^6 is directly proportional to the orientation factor κ^2 for given donor–acceptor species, which means the spatial orientation of the donor and acceptor molecular transition dipoles determine the energy transfer efficiency. Therefore, the almost mutually perpendicular dipole orientation between DSB and Tc/Pc should be not conducive to energy transfer, and κ^2 could be estimated to be 0.004–0.008 as proved in our previous work;[28] but head-to-tail dipole

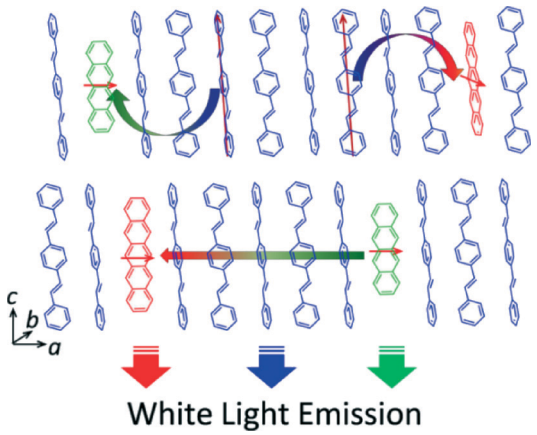

Fig. 5 Proposed molecular stacking of the doubly doped DSB⊂Tc–Pc crystal. The energy transfer processes in the white-light-emission crystal are illustrated by the colored arrows.

orientation should be conductive to energy transfer that occurs between Tc and Pc in the white-emissive DSB⊂Tc–Pc crystal. It is also the reason that the doping concentration of Tc and Pc is approximately 10% (equivalent to shortening the donor–acceptor distance) and that relatively efficient energy transfer between hosts and guests can be achieved, which is attributed to the cross donor–acceptor transition dipole arrangement.

4. Field-effect mobility measurement of white-emissive DSB⊂Tc–Pc crystal

Hole- and electron-transport FETs based on the white-emissive DSB⊂Tc–Pc crystal were constructed, respectively. Gold and calcium electrodes were chosen for the hole- and electron-carrier injections, considering the host DSB HOMO and LUMO levels of ~5.3 and ~2.3 eV, respectively. Fig. 6 shows the output and transfer characteristics of top-contact p- and n-type OFETs based on white-emissive DSB⊂Tc–Pc crystals. Both p- and n-type FET operation was clearly observed under applied negative and positive V_{GS} with a saturated hole mobility of $\mu_h = 1.62 \times 10^{-2}$ cm^2 V^{-1} s^{-1} and a saturated electron mobility of $\mu_e = 2.15 \times 10^{-4}$ cm^2 V^{-1} s^{-1}. As comparison, the pure DSB crystal-based FET was constructed and the hole mobility was measured as ~0.02 cm^2 V^{-1} s^{-1} (see Fig. S4 in the ESI†), which indicates the structural ordering maintenance of the white-emissive DSB⊂Tc–Pc crystal could ensure hole carrier mobility comparable to that of the undoped host. Meanwhile, the electron mobility was two orders of magnitude lower than the hole mobility in the DSB⊂Tc–Pc crystal because the LUMO level of DSB (~2.3 eV) and the work function (WF) of calcium (~2.9 eV) are not well aligned, resulting in poor electron injection. The non-balanced transport of hole- and electron-carriers is unfavourable to realize a white electroluminescence of DSB⊂Tc–Pc crystal using light-emitting FET devices.

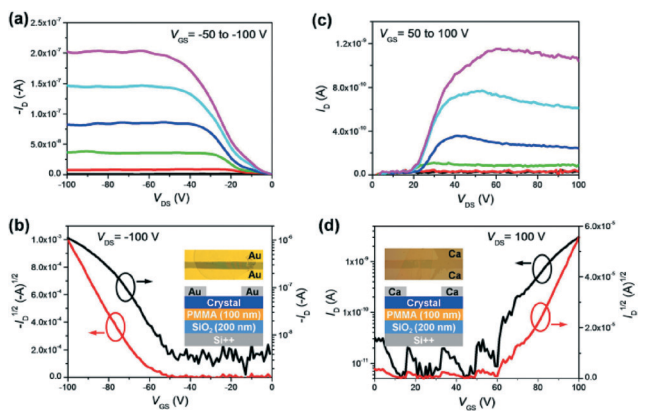

Fig. 6 Output characteristics (a, c) and transfer characteristics (b, d) of OFETs based on white-emissive DSB⊂Tc–Pc crystals with symmetric gold and calcium electrodes, respectively. The insets in figure (b, d) are the device configurations and their top-view photographs. Channel length (L) and width (W) were determined by optical microscopy: L/W = 100/1050 μm (b); L/W = 100/340 μm (d).

Therefore, the preparation of novel host crystalline materials with energy levels matching to the electrode WF, suitable for white-emissive doped organic crystal growth, are the next step for investigation.

5. Chromaticity-stable white-emissive DSB⊂Tc–Pc crystal

The stability of the crystal is considered to be an inherently important characteristic due to the highly ordered and tight arrangement between molecules. For the white-emissive DSB⊂Tc–Pc crystal with the determined mol ratio of host to guest molecules, the intermolecular edge-to-face arene–arene interactions between DSB and Tc/Pc would immobilize their spatial orientations of transition dipoles, which contribute to retain the color stability even under conditions of high-density photon excitation or charge injection. To verify the color stability of the white-emissive DSB⊂Tc–Pc crystal, the photoluminescence properties of the crystal excited with different pumping laser energies have been investigated. A crystal adhered to the quartz substrate was irradiated by the third harmonic (355 nm) of a Nd:YAG (yttrium-aluminum-garnet) laser in the experiment (Fig. 7c shows the crystal photograph under the laser excitation); and the emission spectra were detected by a CCD fiber spectrograph. With the increase of pumping laser energy, the photoluminescence intensity of the white-emissive DSB⊂Tc–Pc crystal increases as shown in Fig. 7a. The crystal emission exhibits good color stability with the CIE coordinates changing from (0.37, 0.39) to (0.32, 0.35) in Fig. 7b as the pumping laser energy is increased from 45 to 1900 kW cm^{-2}. In comparison, a doubly doped DSB⊂Tc–Pc thin film (DSB : Tc : Pc = 300 : 1 : 1) with 300 nm thickness was prepared by vacuum deposition and the thin film emission spectra presented a distinct variation with the pumping laser energy increasing from 12 to 60 kW cm^{-2}, which may be due to the molecular aggregate state change from amorphous to crystalline in the doped thin film induced by the thermal effect of higher laser energy radiation. The emission spectra data of the DSB⊂Tc–Pc thin film is shown in the ESI.† The doped organic crystal, by contrast, has high potential of realizing stable white electroluminescence in organic light-emitting devices.

Conclusions

Large-size and stable white-emissive DSB⊂Tc–Pc crystals with the specific mol ratio of host to guest molecules (DSB : Tc : Pc = 20 : 1 : 0.9) has been prepared by the PVT method. The results of time-resolved fluorescence indicate that the energy transfer occurs not only from the donor DSB to the acceptors Tc and Pc but also from the acceptor Tc to the acceptor Pc in the DSB⊂Tc–Pc crystal. The host DSB matrix upon doping with certain quantities of Tc and Pc molecules retains the structural ordering, as verified by AFM and XRD, which benefits for the carrier transport; and the hole and electron field-effect mobility of the DSB⊂Tc–Pc crystal reaches 1.62×10^{-2} and 2.15×10^{-4} cm^2 V^{-1} s^{-1}, respectively. Compared with the amorphous DSB⊂Tc–Pc film, the crystal emission exhibits

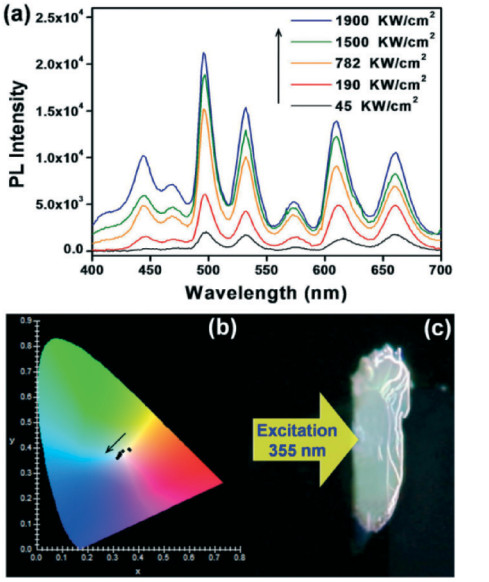

Fig. 7 (a) Photoluminescence spectra of the white-emissive DSB⊂Tc–Pc crystal upon variation of the pumping laser energy. (b) CIE chromaticity diagram marked with the coordinates of (0.37, 0.39), (0.35, 0.38), (0.34, 0.37), (0.33, 0.36) and (0.32, 0.35) corresponding to the crystal emissions excited with the pumping laser energy of 45, 190, 782, 1500 and 1900 kW cm^{-2}, respectively. in (a). (c) Optical photograph of the white-emissive DSB⊂Tc–Pc crystal excited with a 355 nm pumping laser.

better color stability even under the high pumping laser energy excitation. Further developing well-balanced carrier-transport doped organic crystals with high mobility would be promising to realize a stable organic white-lighting crystal device.

Acknowledgements

We are grateful for financial support from the Youth Science Foundation of Heilongjiang Province (QC2014C046), Open Project of State Key Laboratory of Supramolecular Structure and Materials (grant no. sklssm201428).

Notes and references

1 M. Pope, H. P. Kallmann and P. Mangnante, *J. Chem. Phys.*, 1963, **38**, 2042.
2 O. S. Avanesjan, V. A. Benderskii, V. K. Brikenstein, V. L. Broude, L. I. Korshunov, A. G. Lavrushko and I. I. Tartakovskii, *Mol. Cryst. Liq. Cryst.*, 1974, **29**, 165.
3 D. Fichou, S. Delysee and J. M. Nunzi, *Adv. Mater.*, 1997, **9**, 1178.
4 V. Y. Butko, X. Chi and A. P. Ramirez, *Solid State Commun.*, 2003, **128**, 431.
5 A. Dadvand, A. G. Moiseev, K. Sawabe, W. H. Sun, B. Djukic, I. Chung, T. Takenobu, F. Rosei and D. F. Perepichka, *Angew. Chem., Int. Ed.*, 2012, **51**, 3837.
6 Z. Q. Xie, B. Yang, F. Li, G. Cheng, L. L. Liu, G. D. Yang, H. Xu, L. Ye, M. Hanif, S. Y. Liu, D. G. Ma and Y. G. Ma, *J. Am. Chem. Soc.*, 2005, **127**, 14152.
7 H. Yanagi, T. Ohara and T. Morikawa, *Adv. Mater.*, 2001, **13**, 1452.
8 M. Ichikawa, R. Hibino, M. Inoue, T. Haritani, S. Hotta, T. Koyama and Y. Taniguchi, *Adv. Mater.*, 2003, **15**, 213.
9 S. Varghese, S. J. Yoon, S. Casado, R. C. Fischer, R. Wannemacher, S. Y. Park and J. Gierschner, *Adv. Opt. Mater.*, 2014, **2**, 542.
10 V. C. Sundar, J. Zaumseil, V. Podzorov, E. Menard, R. L. Willett, T. Someya, M. E. Gershenson and J. A. Rogers, *Science*, 2004, **303**, 1644.
11 A. L. Briseno, S. C. B. Mannsfeld, M. M. Ling, S. Liu, R. J. Tseng, C. Reese, M. E. Roberts, Y. Yang, F. Wudl and Z. N. Bao, *Nature*, 2006, **444**, 913.
12 T. He, M. Stolte and F. Würthner, *Adv. Mater.*, 2013, **25**, 6951.
13 X. J. Li, Y. X. Xu, F. Li and Y. G. Ma, *Org. Electron.*, 2012, **13**, 762.
14 S. Z. Bisri, T. Takenobu, Y. Yomogida, H. Shimotani, T. Yamao, S. Hotta and Y. Iwasa, *Adv. Funct. Mater.*, 2009, **19**, 1728.
15 T. Komori, H. Nakanotani, T. Yasuda and C. Adachi, *J. Mater. Chem. C*, 2014, **2**, 4918.
16 R. J. Tseng, R. Chan, V. C. Tung and Y. Yang, *Adv. Mater.*, 2008, **20**, 435.
17 Y. J. Zhang, H. L. Dong, Q. X. Tang, S. Ferdous, F. Liu, S. C. B. Mannsfeld, W. P. Hu and A. L. Briseno, *J. Am. Chem. Soc.*, 2010, **132**, 11580.
18 Q. H. Cui, L. Jiang, C. Zhang, Y. S. Zhao, W. P. Hu and J. N. Yao, *Adv. Mater.*, 2012, **24**, 2332.
19 Y. V. Naboikin, L. A. Ogurtsova, A. P. Podgornyi and L. Y. Malkes, *Sov. J. Quantum Electron.*, 1978, **8**, 457.
20 H. S. Avanesyan, V. A. Benderskii, V. K. Brikenshtein, A. G. Lavrushko and P. G. Filippov, *Phys. Status Solidi A*, 1975, **30**, 781.
21 Y. S. Zhao, H. B. Fu, F. Q. Hu, A. D. Peng, W. S. Yang and J. N. Yao, *Adv. Mater.*, 2008, **20**, 79.
22 T. Takenobu, S. Z. Bisri, T. Takahashi, M. Yahiro, C. Adachi and Y. Iwasa, *Phys. Rev. Lett.*, 2008, **100**, 066601.
23 K. Sawabe, M. Imakawa, M. Nakano, T. Yamao, S. Hotta, Y. Iwasa and T. Takenobu, *Adv. Mater.*, 2012, **24**, 6141.
24 H. Wang, F. Li, B. R. Gao, Z. Q. Xie, S. J. Liu, C. L. Wang, D. H. Hu, F. Z. Shen, Y. X. Xu, H. Shang, Q. D. Chen, Y. G. Ma and H. B. Sun, *Cryst. Growth Des.*, 2009, **9**, 4945.
25 C. C. Wu, M. C. Delong, Z. V. Vardeny and J. P. Ferraris, *Synth. Met.*, 2003, **137**, 939.
26 H. M. Cuppen, W. S. Graswinckel and H. Meekes, *Cryst. Growth Des.*, 2004, **4**, 1351.
27 R. Ruiz, D. Choudhary, B. Nickel, T. Toccoli, K. C. Chang, A. C. Mayer, P. Clancy, J. M. Blakely, R. L. Headrick, S. Iannotta and G. G. Malliaras, *Chem. Mater.*, 2004, **16**, 4497.
28 H. Wang, B. L. Yue, Z. Q. Xie, B. R. Gao, Y. X. Xu, L. L. Liu, H. B. Sun and Y. G. Ma, *Phys. Chem. Chem. Phys.*, 2013, **15**, 3527.
29 H. Wang, Y. Zhao, Z. Q. Xie, H. Y. Wang, B. H. Wang and Y. G. Ma, *CrystEngComm*, 2014, **16**, 4539.
30 Z. Q. Xie, W. J. Xie, F. Li, L. L. Liu, H. Wang and Y. G. Ma, *J. Phys. Chem. C*, 2008, **112**, 9066.
31 T. Förster, *Discuss. Faraday Soc.*, 1959, **27**, 7.

32 J. Gierschner, L. Lüer, B. M. Medina, D. Oelkrug and H.-J. Egelhaaf, *J. Phys. Chem. Lett.*, 2013, **4**, 2686.
33 J. M. Robertson, V. C. Sinclair and J. Trotter, *Acta Crystallogr.*, 1961, **14**, 697.
34 R. B. Campbell, J. M. Robertson and J. Trotter, *Acta Crystallogr.*, 1962, **15**, 289.
35 S. H. Lim, T. G. Bjorklund, F. C. Spano and C. J. Bardeen, *Phys. Rev. Lett.*, 2004, **92**, 107402.
36 H. B. Klevens and J. R. Platt, *J. Chem. Phys.*, 1949, **17**, 470.
37 H. Wang, Z. Q. Xie, B. Yang, F. Z. Shen, Y. P. Li and Y. G. Ma, *CrystEngComm*, 2008, **10**, 1252.
38 F. C. Spano, *Annu. Rev. Phys. Chem.*, 2006, **57**, 217.
39 J. Gierschner, M. Ehni, H.-J. Egelhaaf, B. Milián Medina, D. Beljonne, H. Benmansour and G. C. Bazan, *J. Chem. Phys.*, 2005, **123**, 144914.
40 T. Förster, *Ann. Phys.*, 1948, **437**, 55.